HHS Public Access

Author manuscript

Acta Biomater. Author manuscript; available in PMC 2017 July 17.

Published in final edited form as:

Acta Biomater. 2017 April 15; 53: 109–122. doi:10.1016/j.actbio.2017.02.020.

Aspirin-Triggered Resolvin D1-modified materials promote the accumulation of pro-regenerative immune cell subsets and enhance vascular remodeling

Mary Caitlin P. Sok, **Maxianne C. Tria**, **Claire E. Olingy**, **Cheryl L. San Emeterio**, and **Edward A. Botchwey**[*]

Wallace H. Coulter Department of Biomedical Engineering, Georgia Institute of Technology and Emory University, Atlanta, GA 30332, USA

Abstract

Many goals in tissue engineering rely on modulating cellular localization and polarization of cell signaling, including the inhibition of inflammatory infiltrate, facilitation of inflammatory cell egress, and clearance of apoptotic cells. Omega-3 polyunsaturated fatty acid-derived resolvins are gaining increasing recognition for their essential roles in inhibition of neutrophil invasion into inflamed tissue and promotion of macrophage phagocytosis of cellular debris as well as their egress to the lymphatics. Biomaterial-based release of lipid mediators is a largely under-explored approach that provides a method to manipulate local lipid signaling gradients in vivo and direct the recruitment and/or polarization of anti-inflammatory cell subsets to suppress inflammatory signaling and enhance angiogenesis and tissue regeneration. The goal of this study was to encapsulate Aspirin-Triggered Resolvin D1 (AT-RvD1) into a degradable biomaterial in order to elucidate the effects of sustained, localized delivery in a model of sterile inflammation. Flow cytometric and imaging analysis at both 1 and 3 days after injury showed that localized AT-RvD1 delivery was able significantly increase the accumulation of anti-inflammatory monocytes and M2 macrophages while limiting the infiltration of neutrophils. Additionally, cytokine profiling and longitudinal vascular analysis revealed a shift towards a pro-angiogenic profile with increased concentrations of VEGF and SDF-1α, and increased arteriolar diameter and tortuosity. These results demonstrate the ability of locally-delivered AT-RvD1 to increase pro-regenerative immune subpopulations and promote vascular remodeling.

Keywords

Resolvin; Immunomodulation; Innate immunity; Vascular remodeling

[*]Corresponding author at: Department of Biomedical Engineering, Georgia Institute of Technology, 315 Ferst Drive, Atlanta, GA 30332, USA. edward.botchwey@bme.gatech.edu (E.A. Botchwey).

Animal experiment compliance statement: All animal experiments were conducted in accordance with ARRIVE guidelines and the National Institutes of Health guide for the Care and Use of Laboratory Animals.

Disclosures: None.

Appendix A. Supplementary data: Supplementary data associated with this article can be found, in the online version, at http://dx.doi.org/10.1016/j.actbio.2017.02.020.

1. Introduction

Resolvins are a class of bioactive small molecule lipids derived from the omega-3 polyunsaturated fatty acids eicosapentaenoic acid (EPA) and docosahexaenoic acid (DHA) [1]. Resolvins are potent proresolving lipid mediators that act to drive cellular processes toward the resolution of inflammation. Specifically, the D-series resolvins derived from DHA act as endogenous agonists of the cellular receptors GPR/32 and ALX/FPR2, which are broadly expressed in immune cells, including neutrophils, monocytes, macrophages, and lymphocytes, and in certain types of specialized epithelial cells [2–4]. Ligation to these receptors results in a number of different actions, including decreased transendothelial migration of neutrophils, enhancement of macrophage phagocytosis of apoptotic cells and microbes, modulation of cytokine release from macrophages, and stimulation of phagocyte efflux from inflamed tissues, all of which are considered hallmarks of active resolution of inflammation [5]. Treatment with resolvins can be used to promote the resolution of inflammation and healing in many pathological conditions, including bacterial infection, peritonitis, and asthma [6–8]. Additionally, subcutaneous resolvin D2 injections have been shown to increase collateral circulation after ischemic injury [9]. While these studies have been promising, many utilized systemic delivery of resolvins, which limits its bioavailability at the site of inflammation and can result in rapid degradation, requiring multiple injections at high dosages [10,11].

Currently, biomaterial-based delivery systems for localized delivery of resolvins have not widely been developed [12,13]. Others have shown that local delivery of resolvin D1 (RvD1) using a biomaterial wrap can reduce neointimal hyperplasia after vascular injury [14,15], but more exploration is needed to fully characterize the effects of local resolvin delivery in other models. Utilization of biomaterial-mediated delivery of resolvins to areas of injured tissue has the potential to amplify the effect of resolvins produced endogenously during inflammation. Aspirin-Triggered Resolvin D1 (AT-RvD1) is a D-series resolvin that can be produced physiologically when the enzyme cyclooxygenase-2 (COX-2) is acetylated in the presence of aspirin [10]. It possesses the same mechanism of action as RvD1, but due to a conformational change of a hydrogen molecule from (S) to (R) around the seventeenth carbon, can resist rapid degradation by oxidoreductases, resulting in a longer *in vivo* half-life [10,16]. The longer activity of AT-RvD1 *in vivo* makes it an attractive small molecule for incorporation into biomaterials that seek to promote resolution of inflammation and enhance wound healing.

One strategy to promote resolution of inflammation is to modulate the profile and activities of cells involved in the inflammatory response [17–22]. Prevention of excessive neutrophil accumulation enhances wound healing in non-healing diabetic wounds and increases cardiac function after acute myocardial infarction due to reduced release of reactive oxygen species, proinflammatory mediators, and proteases - which resulted in a reduction in tissue damage [23-26]. Though excessive accumulation of neutrophils has been associated with tissue damage, recently a unique subset of neutrophils ($CD49d^{+}VEGFR1^{hi}CXCR4^{hi}$) has been identified that possess the ability to migrate towards a VEGF gradient and actively participate in vascular remodeling [27]. These neutrophils can be identified by their CD49d surface receptor expression. Previously, we have shown that the preferential recruitment of

non-classical “anti-inflammatory” monocytes ($CD45^+CD11b^+$-$Ly6C^{low}$ in mice and $CD14^{low}CD16^+$ in humans) as opposed to classical “inflammatory” monocytes ($CD45^+CD11b^+Ly6C^{hi}$ in mice and $CD14^+CD16^-$ in humans) promotes microvascular network expansion after sterile injury through modulation of the local inflammatory environment [17,28,29]. Following recruitment to inflamed tissue, monocytes may transiently persist in their undifferentiated state or differentiate into macrophages. In addition to tuning monocyte recruitment, modulation of macrophage phenotype has been utilized as a strategy to direct tissue regeneration [30–35]. Macrophages exhibit different phenotypes based on their gene and protein expression profiles, and these phenotypes have distinct effector functions that can drive inflammatory processes or promote tissue regeneration [36–38]. Classically-activated (M1) macrophages that are activated in response to injurious or infectious stimuli are strongly microbicidal, produce reactive nitrogen and oxygen intermediates, and release pro-inflammatory cytokines such as tumor necrosis factor-α (TNF-α), interleukin (IL)-1β, and IL-12 [39–42]. M1 macrophages are implicated in initiating and sustaining inflammation, especially in the context of biomaterial implants, where persistent M1 activation can lead to chronic inflammation and fibrosis [43,44]. In contrast, alternatively activated (M2) macrophages can be activated by canonical antiinflammatory cytokines such as IL-4, IL-10, and IL-13, as well as in response to fungal cells, parasites, and apoptotic cells [38,42,45]. M2 macrophages are in turn considered to generally possess anti-inflammatory actions through the release of cytokines such as IL-10, as well as support angiogenesis and tissue repair [32–34]. Therefore, dual-acting therapies that both suppress damaging inflammation via blockade of excessive neutrophil accumulation acutely and also promote the action of anti-inflammatory, proresolving monocytes and macrophages throughout the progression of inflammation represent a promising strategy to enhance tissue repair after injury.

In this study, we investigate how localized delivery of AT-RvD1 from polymer scaffolds modulates the accumulation of circulating neutrophils and monocytes after injury. We show that AT-RvD1 released from poly(lactic-co-glycolic acid) (PLGA) scaffolds retains the ability to inhibit neutrophil function and increase macrophage activity. Using the murine dorsal skinfold window chamber as a model of sterile inflammation and inflammatory vascular remodeling, we demonstrate that AT-RvD1-loaded PLGA scaffolds decrease the frequency of neutrophils and their infiltration into tissue while simultaneously increasing the frequency of anti-inflammatory $Ly6C^{lo}$ monocytes and CD206+ alternatively activated macrophages. Biomaterial delivery of AT-RvD1 resulted in significantly higher numbers of anti-inflammatory monocytes than a single topical dose of dissolved AT-RvD1 immediately following injury. Additionally, we observed a shift in the peri-implant cytokine profile towards a pro-angiogenic microenvironment. AT-RvD1 materials increased microvascular arteriolar diameter and vascular tortuosity, and increased the density of CD31+ microvasculature. These results indicate that biomaterial delivery of AT-RvD1 can alter the tissue microenvironment after injury to ones that supports resolution of inflammation and tissue regeneration.

2. Materials and methods

2.1. Fabrication of loaded and unloaded polymeric thin films

Films loaded with AT-RvD1 or unloaded were made as previously described [17]. Briefly, PLGA (50:50 DLG 5E – Evonik Industries) was solubilized in dichloromethane using a sonicator at 37 °C until dissolved. Ten μ*g* (100 μL) AT-RvD1 (Cayman Chemical) were added to make AT-RvD1-loaded films. Solutions were cast in Teflon molds, and stored at −20 °C until full organic solvent evaporation was observed. Films were then lyophilized for 24 h. A 1 mm biopsy punch was used to produce films used in studies. The morphology of the films were examined by scanning electron microscopy (SEM). Films were coated with Au for 45 s by a Quorum Q-150T ES sputter coater and imaged with a Hitachi SU8010 field emission scanning electron microscope.

2.2. Quantification ofAT-RvD1 release from PLGA films via High Performance Liquid Chromatography (HPLC) measurements

The *in vitro* release of AT-RvD1 from PLGA films was quantified with HPLC. In the release study, 1 mm diameter films were placed into 200 μL phosphate-buffered saline (PBS) and incubated at 37 °C. At predetermined timepoints, the PBS was removed for analysis and replaced with new PBS. Samples were analyzed with a Shi-madzu UFLC High Performance Liquid Chromatograph (Columbia, MD, USA) equipped with a Shimadzu Premier C18, 5 μm (250 × 4.6 mm) column. AT-RvD1 elution was measured at 8.6 min using a wavelength of 301 nm. Known quantities of AT-RvD1 were used to generate a standard curve relating AT-RvD1 mass to total peak area. Using serial dilutions, we determined that the limit of detection was below 0.5 pg/μL. The total amount of AT-RvD1 in each release sample was calculated using the standard curve.

2.3. In vitro macrophage phagocytosis assay

AT-RvD1-loaded PLGA films and empty PLGA films were placed into 1 mL Dulbecco's modified Eagle medium (Gibco) containing 1 mM sodium pyruvate (Gibco) and 2 mM L-glutamine (Gibco) supplemented with 10% Fetal Bovine Serum (FBS, Gibco) overnight. Conditioned media was added to 1×10^5 RAW264.7 cells (ATCC) cultured in 24-well plates. After one hour of treatment, Fluores-brite® Polychromatic Red latex beads (0.5 um, Polysciences) that were opsonized in 10% FBS for 60 min were added at a ratio of 5:1 beads per cell and were allowed to incubate at 37 °C for 4 h. After incubation, the media was removed and cells were fixed with ice cold methanol for 10 min. Fixed cells were then imaged via brightfield and epifluorescence microscopy to detect both cells and phagocytized latex beads. These images were merged in ImageJ, and the total number of beads internalized by cells were counted.

2.4. Myeloperoxidase activity of neutrophils

MPRO neutrophil progenitor cells (ATCC) were cultured using Iscove's modified Dulbecco's medium (Gibco) containing 10 ng/ml murine granulocyte macrophage colony stimulating factor, 80% and heat-inactivated horse serum, 20%. Terminal granulocytic differentiation of MPRO cells was initiated by replating cells in fresh medium containing 1×10^{-5} M all-trans

Retinoic Acid and culturing for one week to ensure full differentiation. AT-RvD1-loaded PLGA films and empty PLGA films were placed into 1 mL MPRO differentiation medium overnight. Release media was added to 1×10^6 differentiated neutrophils and cells were treated for four hours. Myeloperoxidase (MPO) activity was then measured using a Colorimetric Activity Assay Kit (MAK068, Sigma) according to kit instructions at a sample size of 1×10^5 cells per well.

2.5. Dorsal skin fold window chamber surgery

Animal experiments were performed using sterile techniques in accordance with an approved protocol form the Georgia Institute of Technology Institutional Animal Care and Use Committee. Male C57BL/6 mice (Jackson) aged 6-12 weeks were anesthetized by inhaled isoflurane and surgically fitted with sterile dorsal skinfold window chambers (APJ Trading Co.) as previously described [17]. Briefly, the dorsal skin was shaved, depiliated, and sterilized via three washes with 70% ethanol and chlorhexidine. The dorsal skin was drawn away from the back of the mouse and one side of the titanium frame was attached to the underside of the skin. Sterile surgical micro scissors were then used to expose the microvasculature through the removal of the epidermis and dermis in a 12 mm diameter circle. Mice were implanted with two of the same films (either empty PLGA vehicle film or AT-RvD1-loaded PLGA film) placed on opposite sides of the window chamber. Before implantation, the films were washed in 70% ethanol for 30 s, followed by washing with sterile Ringer's solution for 30 s. Exposed tissue was then sealed with a sterile glass coverslip. Mice were administered sustained-released buprenorphine i.p. (0.1-0.2 mg/kg) and allowed to recover in heated cages. All mice received standard laboratory diet and water ad libitum throughout the course of the experiment.

2.6. Vascular metrics

Mice were anesthetized with isoflurane, the glass window was removed, and dorsal tissue was superfused with adenosine in Ringer's solution (1 mM) to prevent desiccation and to maximally dilate exposed vessels. The mouse was mounted on a microscope stage and imaged non-invasively at 5× magnification on a Zeiss Imager. D2 microscope with AxioCam MRC 5 color digital camera (Zeiss). Images were acquired on day 0 immediately following film implantation and again on day 3. Microvascular length density measurements were made within a 4000 × 4000 pixel square region of interest (ROI) around the film. Vessels within these ROIs were traced and total vessel length per unit area was quantified via ImageJ. Arteriolar diameter measurements were made within the ROIs by identifying arteriolar-venular pairs at day 0. Internal diameter changes were measured via ImageJ and day 3 diameters were normalized to day 0. Vascular tortuosity measurements were made within the ROIs by measuring the distance metric - the path length of a meandering curve divided by the linear distance between end-points in ImageJ.

2.7. Tissue harvest and flow cytometry

To collect samples for flow cytometry analysis, mice were euthanized via CO2 asphyxiation. Peripheral blood was collected via cardiac puncture. Erythrocytes within blood were lysed with ammonium chloride (StemCell Technologies) and the remaining leukocytes were isolated for flow cytometry analysis. Bone marrow was collected via centrifugation (1000g

for 5 min) of isolated tibiae. The dorsal tissue was excised and digested with collagenase type 1-A (1 mg/ml, Sigma) at 37 °C for 30 min and further separated with a cell strainer to create a single cell suspension. Single cell suspensions of tissues, blood, and bone marrow were stained for flow cytometry analysis using standard methods and analyzed on a FACS-AriaIIIu flow cytometer (BD Biosciences). The antibodies used for identifying cell populations of interest were: PerCP-Cy5.5 conjugated anti-CD45 (BioLegend), APC-Cy7 conjugated anti-CD11b (BioLegend), BV421 conjugated anti-CD11b (BioLegend), APC conjugated anti-Ly6C (BioLegend), BV510 conjugated anti-Ly6C (BioLegend), APC-Cy7 conjugated anti-Ly-6G (BioLegend), PE-Cy7 conjugated anti-GR-1 (BioLegend), APC conjugated anti-F4/80 (BioLegend), PE-Cy7 conjugated anti-CD206 (BioLegend), AlexaFluor488 conjugated anti-CD86 (BioLegend), PE conjugated anti-CD49d (BioLegend).

2.8. Tissue whole mount immunohistochemistry and confocal imaging

Following euthanasia, mouse vasculature was perfused with warm saline and then with 4% paraformaldehyde until tissues were fixed. The dorsal tissue was excised and permeabilized overnight at 4 °C with 0.2% saponin. The tissues were blocked overnight in 10% mouse serum at 4 °C. Tissues were incubated at 4 °C overnight in staining solution containing 0.1% saponin, 5% mouse serum, 0.5% fatty-acid free bovine serum albumin, and the following fluorescently conjugated antibodies: Alexa Fluor 594 anti-CD31 antibody (1:100 dilution, BioLegend) for blood vessel visualization, Alexa Fluor 488 anti-Ly-6G (1:200 dilution, BioLegend) for visualization of neutrophils, and Alexa Fluor 647 anti-CD68 (1:200 dilution, ABD Serotec) for visualization of monocytes/macrophages [46]. Tissues were washed four times for 30 min with 0.2% saponin and once with PBS and then mounted in 50/50 glycerol/phosphate buffered saline. Mounted samples were imaged on a Zeiss LSM 710 NLO confocal. Tiled z-stacks at 10× magnification were taken for analysis of CD31+ vasculature. Crops of 1000 × 1000 pixels of background vasculature or peri-implant vasculature were used for measurement of CD31+ length density. For vessel density measurements, vessels were traced and total vessel length per unit area was quantified via ImageJ. Crops of 332 × 332 μm at 20× magnification in the peri-implant area were taken for image analysis in Imaris™ (Bitplane). Images were then blinded and rendered in Imaris by a third party. Cells expressing Ly-6G or CD68 were identified in Imaris using the surface tool. Ly-6G+ or CD68+ surfaces were identified by smoothing with a 1 μm grain size and automatic thresholding on absolute intensity. Touching objects were split using a seed points diameter of 10 μm. CD31+ vasculature was identified in Imaris using the same surface method as described above, also applying a 1 μm grain size, but instead manually selecting the threshold value optimized for each image, and manually applying the volume filter to remove small debris. Distance to vasculature calculations between Ly-6G+ cells and CD31+ vasculature were made by applying a distance transformation to the CD31+ surface and recording the median position of each Ly-6G+ surface relative to CD31+ vessels.

2.9. Cytokine measurements

For cytokine measurements, 4 mm biopsy punches of tissue centered around each biomaterial implant were harvested after euthanasia. Tissue biopsy punches were combined for each animal, digested for 30 min at 37 °C in 1 mg/mL collagenase-type 1A, and

disaggregated through a cell strainer. Protein was isolated from the single cell suspension in RIPA buffer containing Halt™ Protease and Phosphatase Inhibitor Cocktail (diluted to 1×, ThermoFisher Scientific) for 45 min on ice. Following cell lysis, total protein was obtained by centrifugation for 15 min at 14,000g and 4 °C. To determine the total protein concentration in each sample, a bicinchoninic acid assay (BCA assay) was carried out using a Pierce™ BCA Protein Assay Kit (ThermoFisher Scientific) according to kit instructions. Cytokine measurements were made using the Mouse Magnetic Luminex Screening Assay (catalog number LXSAMSM, R&D Systems) according to kit instructions. Kit analytes included CCL2/MCP-1/JE, CXCL12/SDF-1α, FGF-β, G-CSF, GM-CSF, IFN-γ, IGF-1, IL-10, IL-12p70, IL-4, IL-6, MMP-9, TNF-α, and VEGF. Cytokine results were normalized to sample total protein.

2.10. Statistical analysis

All statistical analyses were performed using Graphpad Prism version 6.0 (LaJolla, CA). Results are presented as mean ± standard error of the mean (SEM). For pairwise comparisons, unpaired two-tailed t-tests with Welch's correction, if variance was significantly different, were used. For grouped analyses, one-way ANOVA with Tukey's post-test was used for multiple comparisons. For grouped analyses comparing data over time, two-way ANOVA with Tukey's post-hoc test was used. Unless otherwise noted, $p < 0.05$ was considered statistically significant. For analysis of cellular distance to vasculature, data reflect cells counted from three ROIs acquired across 3-4 animals per group, and statistical comparisons were made using a two-tailed Mann-Whitney test.

3. Results

3.1. PLGA films release bioactive AT-RvD1

PLGA thin films were fabricated to encapsulate and rapidly release encapsulated AT-RvD1. The release of AT-RvD1 was measured through the use of a gradient method via HPLC using a UV-Vis detector at a wavelength of 301 nm. Known concentrations of AT-RvD1 were tested using this method and the retention time was found to be centered around 8.6 min. To assess AT-RvD1 release kinetics, unloaded PLGA films or films loaded with AT-RvD1 were incubated in PBS. The AT-RvD1 peak was detected during analysis of the AT-RvD1 release samples, while no peaks were detected corresponding to this retention time when empty PLGA films were tested (Fig. S1A and B). The AT-RvD1-loaded PLGA films released 1.2 ± 0.2 ng of the loaded AT-RvD1 after 1 h, 7.2 ± 0.3 ng after 24 h, 8.6 ± 0.2 ng after day 3, and 10.3 ± 0.1 ng after day 7 (Fig. S1C and D). Release after 7 days was below the limits of detection. To further characterize the films, scanning electron microscopy was used to observe the surface of the films. No observed differences were seen in the surface morphology of AT-RvD1-loaded or empty PLGA films (S1E-F).

After we verified release of AT-RvD1 from PLGA films, the bioactivity of released AT-RvD1 was assessed. Previous studies have shown that exposure to resolvins increase macrophage phagocytic ability, therefore a phagocytosis assay was used to confirm At-RvD1 bioactivity after release from PLGA films [47]. Cell culture media was incubated with AT-RvD1-loaded PLGA films or empty PLGA films AT-RvD1 for 24 h and then used to

treat RAW264.7 macrophages. Based on HPLC measurements, the films released an average of 7.5 ± 0.6 ng AT-RvD1 into RAW264.7 cell culture media over 24 h. After 4 h of treatment, phagocytic ability was measured using fluorescent latex beads. RAW264.7 macrophages that were treated with media containing released AT-RvD1 exhibited increased phagocytosis of latex beads, as visualized using fluorescence microscopy (Fig. 1A and B). Quantification of the number of phagocytosed latex beds indicated increases in the overall phagocytic activity of macrophages treated with AT-RvD1 film release media (Fig. 1C). As a secondary metric of bioactivity, we treated MPRO neutrophils with release media derived from AT-RvD1 films. Neutrophils treated with media incubated with AT-RvD1-loaded PLGA films exhibited significantly decreased MPO activity after both 30 and 60 min compared to neutrophils treated with media incubated with unloaded PLGA films (Fig. 1D). Taken together, these results demonstrate that AT-RvD1 maintains its bioactivity after release from PLGA films and promotes myeloid cell functions induced by native AT-RvD1.

3.2. AT-RvD1 delivery decreases neutrophil infiltration in the acute phases of inflammation

To explore myeloid cell influx during the inflammatory cascade, the murine dorsal skinfold window chamber model was used. This model allows for longitudinal intravital imaging of host responses to biomaterial implants including remodeling of microvascular networks and changes to the innate immune response following injury and material implantation [17,28,29]. To evaluate the in vivo infiltration of circulating neutrophils, we utilized whole mount immunohistochemistry (IHC) and flow cytometry at days 1 and 3 after implantation of AT-RvD1-loaded PLGA or unloaded PLGA onto the dorsal tissue. For initial analysis, an additional group consisting of 100 ng AT-RvD1dissolved in 200 μL sterile saline was added to compare the effects of one-time bolus delivery with biomaterial-mediated delivery. This dosage was chosen based on previous studies utilizing AT-RvD1 [16]. Neutrophils were immunophenotyped as $CD45^+CD11b^+Ly\text{-}6C^+Ly\text{-}6G^+$ [48]. At day 1, neutrophils were the dominating cell type present out of all $CD45^+$-$CD11b^+$ myeloid cells. In the tissue, animals treated with AT-RvD1 scaffolds and saline–AT–RvD1 solution had a significantly lower frequency of neutrophils compared to animals that received unloaded PLGA scaffolds (Fig. 2A). This decrease in neutrophils present in the tissue was accompanied by a significant increase in the neutrophil frequency within the blood of AT-RvD1-treated mice, but not in mice receiving the saline-AT-RvD1 solution (Fig. 2B). All groups undergoing dorsal skinfold window chamber surgery demonstrated elevation of blood neutrophils relative to uninjured control animals; however, neutrophils were even further elevated in the AT-RvD1 scaffold group (Fig. 2C). By day 3, there were no differences in tissue or blood neutrophils in either group, but the overall proportion of neutrophils out of all $CD45^+CD11b^+$ cells decreased greatly, likely due to the influx of $CD45^+CD11b^+$ monocytes (Fig. S2A and B). After 1 day, the proportion of pro-angiogenic neutrophils expressing CD49d remained unchanged between animals given AT-RvD1-loaded implants and PLGA-only implants in both blood and tissue (Fig. 2D and E). However, after three days there were significantly more CD49d+ neutrophils present in the tissue of animals treated with AT-RvD1 scaffolds, but no differences were observed in the blood (Fig. 2F and G).

Qualitative confocal micrographs taken 24 h after surgery reveal a larger number of Ly-6G+ neutrophils in the tissue of mice treated with control PLGA films compared to AT-RvD1

film treated animals (Fig. 2H and I). A 3D transformation representing the distance from $CD31^+$ vasculature was overlaid onto Imaris-rendered images to analyze the distance that neutrophils had invaded into the extravascular tissue space (Fig. 3A–D). Neutrophils in the peri-implant area of PLGA-only scaffolds were able to migrate significantly further into the interstitial tissue than neutrophils in the peri-implant area of AT-RvD1-loaded PLGA scaffolds after 1 day post-injury (Fig. 3C). However, no difference was found in neutrophil migration through interstitial tissue after 3 days (Fig. 3D). Additionally, 3D analysis of total cell numbers revealed that tissue surrounding AT-RvD1 implants have significantly fewer Ly-$6G^+$ neutrophils at both days 1 and 3 after scaffold implantation (Fig. 3E and F). Collectively, these data suggest that local release of AT-RvD1 can suppress neutrophil infiltration and migration in the early stages of inflammation.

3.3. AT-RvD1 increases anti-inflammatory monocyte and macrophage populations

In addition to exploring the effect of local AT-RvD1 on neutrophil infiltration, we examined the accumulation of monocyte and macrophage subsets after injury to the dorsal skin. After 3 days, 3D renderings show more CD68+ monocytes/macrophages in the peri-implant tissue of mice treated with AT-RvD1-loaded scaffolds (Fig. 4A and B). Following quantification, AT-RvD1-treated animals were found to have significantly more CD68+ monocytes/macrophages than PLGA-only animals (Fig. 4C). Further analysis of 3D renderings reveals a significantly lower neutrophil-to-monocyte/macrophage ratio in animals treated with AT-RvD1 scaffolds compared to animals that received unloaded PLGA scaffolds (Fig. 4D). An increase in the ratios of neutrophils to other subsets of white blood cells have been associated with persistent inflammation and poor clinical outcomes in malignancy and wound healing [49–51].

In order to further examine the hypothesis that biomaterial-delivered AT-RvD1 can influence the accumulation of anti-inflammatory immune cells, we performed flow cytometry to further characterize myeloid cell subpopulations present in the inflamed dorsal tissue. Analysis 1 day after injury indicated that there were no differences in $CD45^+CD11b^+Ly\text{-}6C^{Lo}$ anti-inflammatory monocytes (AM) or $CD45^+CD11b^+Ly\text{-}6C^{Hi}$ inflammatory monocytes (IM) in the tissue for all groups (Fig. S3A and B). After 3 days, there were significantly more AMs present in dorsal tissue that had received an AT-RvD1-loaded implant compared to the PLGA only group or a topical dose of AT-RvD1 in solution immediately following surgery (Fig. 5A). Conversely, there were significantly fewer IMs present in the AT-RvD1 treated dorsal tissue compared to PLGA-only and topical AT-RvD1 treatments (Fig. 5B). The ratio of AM to IM in the dorsal tissue was significantly higher in the AT-RvD1 film-treated animals than in AT-RvD1 topical application or empty PLGA implant-treated animals (Fig. 5C). We next immunophenotyped subpopulations of macrophages to explore how AT-RvD1 delivery impacts macrophage accumulation. No differences were found in the frequency of total macrophages between AT-RvD1-loaded PLGA implants and PLGA-only implants after 1 day (Fig. S3C and D). Analysis of digested dorsal tissue after 3 days showed that there was a significant increase in the presence of F4/80+CD86-CD206+ macrophages, an immunophenotype indicative of M2 or alternatively activated macrophages [45], in the AT-RvD1 treated mice (Fig. 5D). The proportion of M1 classically activated F4/80+CD86+CD206- macrophages showed a trend of decrease (Fig.

5E); however, the ratio of M2 to M1 macrophages was significantly increased in animals treated with AT-RvD1-loaded implants. Increases in the ratio of M2 to M1 macrophages have been correlated with increased tissue healing and has consequently been called the "regenerative ratio" [33] (Fig. 5F). Taken together, this data shows that local AT-RvD1 treatment both increases the overall frequency of macrophages present in inflamed dorsal tissue after 3 days and induces accumulation of monocyte and macrophage subsets that have been associated with tissue regeneration and wound healing.

3.4. AT-RvD1 modulates cytokine expression levels in dorsal tissue

To better understand how AT-RvD1 delivery impacts the production of inflammatory mediators, multiplexed protein analysis was performed on peri-implant dorsal tissue both 1 and 3 days post-surgery. The expression levels of known pro-angiogenic and anti-inflammatory cytokines were significantly increased both 1 and 3 days after surgery. There was an increase in the level of VEGF in the At-RvD1 implant tissue after 1 day compared to PLGA implant tissue, which decreased for both groups by day 3 (Fig. 6A). IL-4 expression levels were significantly increased at both day 1 and day 3 in AT-RvD1 implant tissue, but day 3 expression in AT-RvD1 treated animals was decreased compared to day 1 levels (Fig. 6B) and the level of SDF-1α was significantly increased at day 3 in animals treated with AT-RvD1 implants (Fig. 6C). Expression levels of other proteins such as MMP-9 and FGF-b were unchanged between AT-RvD1-implant and PLGA implant animals (Fig. S4A and B). Levels of IL-10 were found to be no different between AT-RvD1-implant and PLGA implant animals after 1 day, but all samples had IL-10 levels below the limit of detection at day 3 (Fig. S4C).

3.5. AT-RvD1 enhances microvascular remodeling

In order to determine if the local delivery of AT-RvD1 to injured tissue promotes expansion and remodeling of microvascular networks, brightfield imaging of window chambers was conducted after material implantation (day 0) and again at day 3 after injury (Fig. 7A–D). Micrographs were then assessed for changes in the vascular parameters of total length, arteriolar diameter, and vascular tortuosity, all of which are classic signs of microvascular remodeling [28]. The total length of vasculature normalized to the area of analysis (i.e. length density) was unchanged between groups after 3 days (Fig. 7E). Conversely, a significant increase in both the arteriolar diameter and vascular tortuosity of AT-RvD1-treated animals was observed compared to animals receiving PLGA-only implants (Fig. 7F and G). These changes to the vasculature can be observed in the micrographs of AT-RvD1 treatment (Fig. 7D), and are absent in the peri-implant area of PLGA-only scaffolds (Fig. 7B). While we were unable to discern differences in vascular length density using brightfield imaging, we have previously demonstrated that whole mount CD31 immunostaining can reveal changes to capillary-level microcirculation that is undetectable by brightfield microscopy [29]. Whole mount confocal images of both background tissue away from the biomaterial implant and peri-implant CD31+ immunostained vessels revealed small vessels that were not observable with brightfield microscopy (Fig. 8A–D). Analysis of CD31 length per unit area at one day after surgery revealed no differences in length density between background and peri-implant area in animals receiving AT-RvD1-loaded or empty PLGA implants (Fig. 8E). However, at day 3, AT-RvD1 delivery from PLGA films significantly

increased the density of CD31+ vessels near the implant compared to background and also compared to PLGA-only implant in the window chamber (Fig. 8F).

4. Discussion

Acute inflammation is a protective response mounted by the host after injury and/or infection [52]. During acute inflammation, polymorphonuclear neutrophils are recruited to the site of inflammation through the expression of pathogen- or damage-associated molecular patterns [53–55]. These neutrophils, along with activated tissue resident macrophages, trigger the sequential release of proinflammatory mediators such as eicosanoids, cytokines, chemokines, and proteases, and these mediators drive leukocyte recruitment and activation [56–58]. In the case of a minor injury or infection, the acute inflammatory response will subside and return to homeostasis via the active process of inflammation resolution, signified by diminished number and activity of neutrophils and macrophage phenotype switching, phagocytosis, and egress [59,60]. However, in large wounds or in diseases such as arthritis or atherosclerosis, acute inflammation may continue unabated and progress to chronic inflammation, where persistent accumulation and activation of neutrophils and mononuclear cells results in fibrosis and tissue damage [61–64]. In the field of biomaterials and tissue engineering, inflammation that is allowed to continue unabated can impair host-implant integration and tissue regeneration, leading to implant failure [65–68]. Therefore, balancing processes of inflammation and resolution are vital to ensuring the success of biomaterial and tissue engineered scaffolds. Here, we utilized a locally-delivered dual-acting lipid mediator to regulate active inflammatory processes and drive resolution by inhibiting neutrophil infiltration and increasing the presence of anti-inflammatory monocytes and macrophages.

Resolvins are in a class of molecules that have been deemed specialized pro-resolving mediators that are produced during the acute inflammatory response. Their actions drive the restoration of tissue homeostasis and prevention of fibrosis after the acute inflammatory response through a dual anti-inflammatory pro-resolution mechanism by which the activities of pro-inflammatory cells are dampened and those of anti-inflammatory cells are enhanced [8]. Currently, there are many studies investigating resolvins for various therapeutic applications that seek to leverage their pro-resolving function. For example, intravenous AT-RvD1 can suppress inflammatory responses and protects against kidney injury in a murine model of acute kidney injury [69]. Additionally, RvD1 can modulate human and murine T cell differentiation, while enhancing the generation of T-regulatory cells [70]. While these studies have shown promising therapeutic uses for AT-RvD1, little exploration has been done into the utilization of biomaterials to locally deliver AT-RvD1 to areas of inflammation after injury. We have shown here for the first time that sustained delivery of AT-RvD1 from PLGA scaffolds over several days results in differences in myeloid cell accumulation to skin after injury compared to a one-time dose of dissolved AT-RvD1. The dosage of AT-RvD1 delivered via topical saline was 100 ng, while 10.2 ng AT-RvD1 on average were loaded into each biomaterial film. We found that both biomaterial-delivered AT-RvD1 and AT-RvD1 solution were able to significantly reduce neutrophil infiltration after one day, but only AT-RvD1-loaded scaffolds were able to increase $Ly6C^{lo}$ AMs, while decreasing $Ly6C^{hi}$ IMs after three days, indicating that sustained release at a lower dose is better able to modulate

the cellular response after injury (Figs. 2A and B, 5A– C). These findings motivated us to investigate further how local delivery of AT-RvD1 via a biomaterial is able to modulate inflammation and promote tissue regeneration.

In the process of wound healing without infection, it was previously believed that neutrophils had little to no bearing on the outcome of tissue repair [71]. However, recent studies exploring the role of neutrophils in wound healing have shown that excessive neutrophil infiltration into tissue can impair repair through the release of neutrophil extracellular traps (NETs), reactive oxygen species (ROS) and proteolytic enzymes, specifically in the context of diabetes and post-myocardial infarction cardiac remodeling [23,25,26,71–73]. Excessive neutrophil recruitment and persistent activation is associated with chronic inflammation, fibrosis, and poor healing [74–76]. Additionally, targeted depletion of neutrophils in mice has been found to accelerate wound closure [77,78]. High neutrophil counts in relation to lymphocytes and macrophages have also been clinically associated with poor outcomes in a number of diseases, including colon cancer and atherosclerosis [79,80]. For instance, patients with an elevated neutrophil to lymphocyte ratio are more likely to experience cardiac death and mortality after acute myocardial infarction [73,81], and mice with pancreatic cancer that have an elevated neutrophil-to-macrophage ratio are more likely to develop severe ascites or bowel obstruction [50]. In the present study, we demonstrate reduced neutrophils present at one day after injury in mice treated with AT-RvD1-loaded films via flow cytometry and quantification of whole mount IHC. Resolvins have been shown to block neutrophil transendothelial migration through inhibition of neutrophil chemotaxis towards cytokine gradients created during the inflammatory process [82]. Neutrophil levels were elevated in the blood but reduced in tissue, and neutrophils that did migrate into the tissue were unable to infiltrate further through the tissue. These data suggest that the local delivery of AT-RvD1 can not only block transendothelial migration of neutrophils as has been demonstrated previously via systemic treatment with resolvins, but can also prevent further tissue damage by inhibiting neutrophil migration through the interstitial tissue (Figs. 2 and 3). Animals treated with AT-RvD1 also had a lower neutrophil-to-monocyte/ macrophage ratio at 3 days after surgery, and we propose that this metric can be used to indicate a positive correlation to inflammation resolution and the prevention of chronic inflammation.

During tissue regeneration, the remodeling and expansion of wound-associated vasculature is critical to ensure tissue oxygenation, nutrient delivery, and cell recruitment [29]. Recently, a newly discovered subset of neutrophils has been described that stimulate angiogenesis in response to VEGF [27]. We have found that CD49d+ neutrophils accumulate in injured dorsal tissue three days after treatment with AT-RvD1-loaded films (Fig. 2F), and these neutrophils can actively participate in vascular remodeling and network expansion. We have previously shown that the recruitment of $Ly6C^{lo}$ AMs using SDF-1α-loaded hydrogels or FTY720-releasing films is associated with increased angiogenesis and arteriogenesis during inflammation [17,28,29]. Here we have shown that the local delivery of AT-RvD1 is able to enhance accumulation of AMs in the dorsal tissue as early as three days after surgery (Fig. 4). In addition to increasing the ratio of AMs to IMs, M2 alternatively activated macrophages were also increased in the tissue of AT-RvD1-loaded film-treated animals (Fig. 5). These specific subsets of monocytes and macrophages are able to directly influence

vascular remodeling [83–85], and increased AM/IM and M2/M1 ratios are associated with enhanced tissue regeneration and healing [29,33]. The mechanisms of these observed increases in anti-inflammatory subsets of monocytes and macrophages could be a result of increased monocyte recruitment from circulation. Alternatively, AT-RvD1 may alter in situ monocyte/macrophage polarization towards AM/M2 due to direct action by AT-RvD1 on macrophages or through external factors, such as phagocytosis of apoptotic neutrophils [86]. Local AT-RvD1 delivery was also able to modulate the peri-implant cytokine profile towards a pro-angiogenic/arteriogenic environment, with significant elevation in VEGF, SDF-1α, and IL-**4**, cytokines that contribute to vascular remodeling and the recruitment of cells that participate in vascular remodeling (Fig. 6) [87–90]. Indeed, the enhanced arteriolar diameter and vascular tortuosity we observed with brightfield microscopy and expansion of microvasculature observed with confocal imaging 3 days after implantation are early hallmarks of sustained arteriogenesis and vascular remodeling (Fig. 7).

5. Conclusions

Taken together, localized delivery of AT-RvD1 allows for dual targeting of both pro-inflammatory and pro-regenerative cells involved in inflammation and wound healing. Modulation of initial neutrophil infiltration allows for reduced overall tissue damage and primes the tissue for regeneration and healing. Enhanced accumulation of anti-inflammatory monocyte and macrophage cell subsets further reduce inflammation and promote early tissue regeneration and vasculogenesis. These results establish localized delivery of AT-RvD1 as a promising approach to modulate the innate immune response to reduce tissue damage associated with excessive inflammation and promote therapeutic outcomes such as vascular remodeling.

Supplementary Material

Refer to Web version on PubMed Central for supplementary material.

Acknowledgments

We thank the core facilities staff of the Parker H. Petit Institute for Bioengineering and Bioscience for technical expertise and assistance (particularly Andrew Shaw and Nadia Bugoslavsky), the Physiological Research Lab staff for guidance on *in vivo* studies, and the Emory University Integrated Cellular Imaging Microscopy Core for their expertise and assistance in image analysis.

Sources of funding: Sources of support for this study include the National Institutes of Health grants K01AR052352-01A1, R01AR056445-01A2, and R01DE019935-01 to Dr. Botchwey.

References

1. Serhan CN, Petasis NA. Resolvins and protectins in inflammation resolution. Chem Rev. 2011; 111(10):5922–5943. [PubMed: 21766791]
2. Ho KJ, Spite M, Owens CD, Lancero H, Kroemer AHK, Pande R, Creager MA, Serhan CN, Conte MS. Aspirin-triggered lipoxin and resolvin E1 modulate vascular smooth muscle phenotype and correlate with peripheral atherosclerosis. Am J Pathol. 2010; 177(4):2116–2123. [PubMed: 20709806]

3. Miyahara T, Runge S, Chatterjee A, Chen M, Mottola G, Fitzgerald JM, Serhan CN, Conte MS. D-series resolvin attenuates vascular smooth muscle cell activation and neointimal hyperplasia following vascular injury. FASEB J. 2013; 27(6):2220–2232. [PubMed: 23407709]

4. Clària J, Nguyen BT, Madenci AL, Ozaki CK, Serhan CN. Diversity of lipid mediators in human adipose tissue depots. Am J Physiol Cell Physiol. 2013; 304(12):C1141–9. [PubMed: 23364264]

5. Spite M, Clària J, Serhan CN. Resolvins, specialized proresolving lipid mediators, and their potential roles in metabolic diseases. Cell Metab. 2014; 19(1):21–36. [PubMed: 24239568]

6. Norling LV, Spite M, Yang R, Flower RJ, Perretti M, Serhan CN. Cutting edge: humanized nano-proresolving medicines mimic inflammation-resolution and enhance wound healing. J Immunol. 2011; 186(10):5543–5547. [PubMed: 21460209]

7. Ortega Gómez A, Perretti M, Soehnlein O. Resolution of inflammation: an integrated view. EMBO Mol Med. 2013; 5(5):661–674. [PubMed: 23592557]

8. Levy BD. Resolvins and protectins: natural pharmacophores for resolution biology. Prostaglandins Leukot Essent Fatty Acids. 2010; 82(4):327–332. [PubMed: 20227865]

9. Zhang MJ, Sansbury BE, Hellmann J, Baker JF, Guo L, Parmer CM, Prenner JC, Conklin DJ, Bhatnagar A, Creager MA, Spite M. Resolvin D2 enhances postischemic revascularization while resolving inflammation. Circulation. 2016; 134(9):666–680. [PubMed: 27507404]

10. Sun YP, Oh SF, Uddin J, Yang R, Gotlinger K, Campbell E, Colgan SP, Petasis NA, Serhan CN. Resolvin D1 and its aspirin-triggered 17R epimer. Stereochemical assignments, anti-inflammatory properties, and enzymatic inactivation. J Biol Chem. 2007; 282(13):9323–9334. [PubMed: 17244615]

11. Tiwari G, Tiwari R, Sriwastawa B, Bhati L, Pandey S, Pandey P, Bannerjee SK. Drug delivery systems: an updated review. Int J Pharm Invest. 2012; 2(1):2–11.

12. Vasconcelos DP, Costa M, Amaral IF, Barbosa MA, Águas AP, Barbosa JN. Development of an immunomodulatory biomaterial: using resolvin D1 to modulate inflammation. Biomaterials. 2015; 53:566–573. [PubMed: 25890752]

13. Kamaly N, Fredman G, Subramanian M, Gadde S, Pesic A, Cheung L, Fayad ZA, Langer R, Tabas I, Farokhzad OC. Development and in vivo efficacy of targeted polymeric inflammation-resolving nanoparticles. PNAS. 2013; 110(16):6506–6511. [PubMed: 23533277]

14. Wu B, Mottola G, Chatterjee A, Lance KD, Chen M, Siguenza IO, Desai TA, Conte MS. Perivascular delivery of resolvin D1 inhibits neointimal hyperplasia in a rat model of arterial injury. J Vasc Surg. 2017; 65(1):207–217. [PubMed: 27034112]

15. Lance KD, Chatterjee A, Wu B, Mottola G, Nuhn H, Lee PP, Sansbury BE, Spite M, Desai TA, Conte MS. Unidirectional and sustained delivery of the proresolving lipid mediator resolvin D1 from a biodegradable thin film device. J Biomed Mater Res. 2017; 105(1):31–41.

16. Rogerio AP, Haworth O, Croze R, Oh SF, Uddin M, Carlo T, Pfeffer MA, Priluck R, Serhan CN, Levy BD. Resolvin D1 and aspirin-triggered resolvin D1 promote resolution of allergic airways responses. J Immunol. 2012; 189(4):1983–1991. [PubMed: 22802419]

17. Awojoodu AO, Ogle ME, Sefcik LS, Bowers DT, Martin K, Brayman KL, Lynch KR, Peirce-Cottler SM, Botchwey E. Sphingosine 1-phosphate receptor 3 regulates recruitment of anti-inflammatory monocytes to microvessels during implant arteriogenesis. Proc Natl Acad Sci USA. 2013; 110(34):13785–13790. [PubMed: 23918395]

18. Wieghaus KA, Capitosti SM, Anderson CR, Price RJ, Price RJ, Blackman BR, Brown ML, Botchwey EA. Small molecule inducers of angiogenesis for tissue engineering. Tissue Eng. 2006; 12(7):1903–1913. [PubMed: 16889520]

19. Sefcik LS, Aronin CEP, Awojoodu AO, Shin SJ, Mac Gabhann F, MacDonald TL, Wamhoff BR, Lynch KR, Peirce SM, Botchwey EA. Selective activation of sphingosine 1-phosphate receptors 1 and 3 promotes local microvascular network growth. Tissue Eng Part A. 2011; 17(5):617–629. [PubMed: 20874260]

20. Das A, Segar C, Hughley BB, Bowers DT, Botchwey EA. The Promotion of Mandibular Defect Healing by the Targeting of S1P Receptors and the Recruitment of Alternatively Activated Macrophages. 2013; 34(38):9853–9862.

21. Das A, Tanner S, Barker DA, Green D, Botchwey EA. Delivery of S1P receptor-targeted drugs via biodegradable polymer scaffolds enhances bone regeneration in a critical size cranial defect. J Biomed Mater Res. 2014; 102(4):1210–1218.
22. Huang C, Das A, Tholpady S, Wang T, Cui Q, Ogle R, Botchwey E. Local delivery of FTY720 accelerates cranial allograft incorporation and bone formation. Cell Tissue Res. 2011; 347(3):553–566. [PubMed: 21863314]
23. Wong SL, Demers M, Martinod K, Gallant M, Wang Y, Goldfine AB, Kahn CR, Wagner DD. Diabetes primes neutrophils to undergo NETosis, which impairs wound healing. Nat Med. 2015; 21(7):815–819. [PubMed: 26076037]
24. Liehn EA, Tuchscheerer N, Kanzler I, Drechsler M, Fraemohs L, Schuh A, Koenen RR, Zander S, Soehnlein O, Hristov M, Grigorescu G, Urs AO, Leabu M, Bucur I, Merx MW, Zernecke A, Ehling J, Gremse F, Lammers T, Kiessling F, Bernhagen J, Schober A, Weber C. Double-edged role of the CXCL12/CXCR4 axis in experimental myocardial infarction. J Am Coll Cardiol. 2011; 58(23):2415–2423. [PubMed: 22115649]
25. Carbone F, Nencioni A, Mach F, Vuilleumier N, Montecucco F. Pathophysiological role of neutrophils in acute myocardial infarction. Thromb Haemost. 2013; 110(3):501–514. [PubMed: 23740239]
26. Vinten-Johansen J. Involvement of neutrophils in the pathogenesis of lethal myocardial reperfusion injury. Cardiovasc Res. 2004; 61(3):481–497. [PubMed: 14962479]
27. Massena S, Christoffersson G, Vagesjo E, Seignez C, Gustafsson K, Binet F, Herrera Hidalgo C, Giraud A, Lomei J, Westrom S, Shibuya M, Claesson-Welsh L, Gerwins P, Welsh M, Kreuger J, Phillipson M. Identification and Characterization of VEGF-A-Responsive Neutrophils Expressing CD49d, VEGFR1, and CXCR4 in Mice and Humans. 2015; 126(17):2016–2026.
28. Ogle ME, Sefcik LS, Awojoodu AO, Chiappa NF, Lynch K, Peirce-Cottler S, Botchwey EA. Engineering in vivo gradients of sphingosine-1-phosphate receptor ligands for localized microvascular remodeling and inflammatory cell positioning. Acta Biomater. 2014; 10(11):4704–4714. [PubMed: 25128750]
29. Krieger JR, Ogle ME, McFaline-Figueroa J, Segar CE, Temenoff JS, Botchwey EA. Spatially localized recruitment of anti-inflammatory monocytes by SDF-1a-releasing hydrogels enhances microvascular network remodeling. Biomaterials. 2016; 77:280–290. [PubMed: 26613543]
30. Spiller KL, Anfang RR, Spiller KJ, Ng J, Nakazawa KR, Daulton JW, Vunjak-Novakovic G. The role of macrophage phenotype in vascularization of tissue engineering scaffolds. Biomaterials. 2014; 35(15):4477–4488. [PubMed: 24589361]
31. Spiller KL, Nassiri S, Witherel CE, Anfang RR, Ng J, Nakazawa KR, Yu T, Vunjak-Novakovic G. Sequential delivery of immunomodulatory cytokines to facilitate the M1-to-M2 transition of macrophages and enhance vascularization of bone scaffolds. Biomaterials. 2015; 37:194–207. [PubMed: 25453950]
32. Hsu CW, Poché RA, Yosef N, Scott L, Vadakkan TJ, Larina IV, West JL. Improved angiogenesis in response to localized delivery of macrophage-recruiting molecules. PLoS One. 2015; 10(7):e0131643. [PubMed: 26132702]
33. Mokarram N, Merchant A, Mukhatyar V, Patel G, Bellamkonda RV. Effect of modulating macrophage phenotype on peripheral nerve repair. Biomaterials. 2012; 33(34):8793–8801. [PubMed: 22979988]
34. Reeves ARD, Spiller KL, Freytes DO, Vunjak-Novakovic G, Kaplan DL. Controlled release of cytokines using silk-biomaterials for macrophage polarization. Biomaterials. 2015; 73:272–283. [PubMed: 26421484]
35. Bartneck M, Heffels KH, Pan Y, Bovi M, Zwadlo-Klarwasser G, Groll J. Inducing healing-like human primary macrophage phenotypes by 3D hydrogel coated nanofibers. Biomaterials. 2012; 33(16):4136–4146. [PubMed: 22417617]
36. Ogle ME, Sridhar S, Segar C, Sridhar S, Botchwey EA, Botchwey EA. Monocytes and macrophages in tissue repair: implications for immunoregenerative biomaterial design. Exp Biol Med (Maywood). 2016; 241(10):1084–1097. [PubMed: 27229903]

37. Arnold L, Henry A, Poron F, Baba-Amer Y, van Rooijen N, Plonquet A, Gherardi RK, Chazaud B. Inflammatory monocytes recruited after skeletal muscle injury switch into antiinflammatory macrophages to support myogenesis. J Exp Med. 2007; 204(5):1057–1069. [PubMed: 17485518]
38. Mosser DM, Edwards JP. Exploring the full spectrum of macrophage activation. Nat Rev Immunol. 2008; 8(12):958–969. [PubMed: 19029990]
39. van Furth R, Cohn ZA. The origin and kinetics of mononuclear phagocytes. J Exp Med. 1968; 128(3):415–435. [PubMed: 5666958]
40. Martinez FO, Gordon S. The M1 and M2 paradigm of macrophage activation: time for reassessment. F1000Prime Rep. 2014; 6(13):13. [PubMed: 24669294]
41. Mantovani A, Sozzani S, Locati M, Allavena P, Sica A. Macrophage polarization: tumor-associated macrophages as a paradigm for polarized M2 mononuclear phagocytes. Trends Immunol. 2002; 23(11):549–555. [PubMed: 12401408]
42. Edwards JP, Zhang X, Frauwirth KA, Mosser DM. Biochemical and functional characterization of three activated macrophage populations. J Leukoc Biol. 2006; 80(6):1298–1307. [PubMed: 16905575]
43. Lech M, Anders HJ. Macrophages and fibrosis: How resident and infiltrating mononuclear phagocytes orchestrate all phases of tissue injury and repair. Biochim Biophys Acta. 2013; 1832(7):989–997. [PubMed: 23246690]
44. Sindrilaru A, Peters T, Wieschalka S, Baican C, Baican A, Peter H, Hainzl A, Schatz S, Qi Y, Schlecht A, Weiss JM, Wlaschek M, Sunderkötter C, Scharffetter-Kochanek K. An unrestrained proinflammatory M1 macrophage population induced by iron impairs wound healing in humans and mice. J Clin Invest. 2011; 121(3):985–997. [PubMed: 21317534]
45. Gordon S, Martinez FO. Alternative activation of macrophages: mechanism and functions. Immunity. 2010; 32(5):593–604. [PubMed: 20510870]
46. Bruce AC, Kelly-Goss MR, Heuslein JL, Meisner JK, Price RJ, Peirce SM. Monocytes are recruited from venules during arteriogenesis in the murine spinotrapezius ligation model. Arterioscler Thromb Vasc Biol. 2014; 34(9) ATVBAHA.114.303399–2022.
47. Krishnamoorthy S, Recchiuti A, Chiang N, Yacoubian S, Lee CH, Yang R, Petasis NA, Serhan CN. Resolvin D1 binds human phagocytes with evidence for proresolving receptors. PNAS. 2010; 107(4):1660–1665. [PubMed: 20080636]
48. Mircescu MM, Lipuma L, van Rooijen N, Pamer EG, Hohl TM. Essential role for neutrophils but not alveolar macrophages at early time points following Aspergillus fumigatus infection. J Infect Dis. 2009; 200(4):647–656. [PubMed: 19591573]
49. Hasegawa S, Eguchi H, Tomokuni A, Tomimaru Y, Asaoka T, Wada H, Hama N, Kawamoto K, Kobayashi S, Marubashi S, Konnno M, Ishii H, Mori M, Doki Y, Nagano H. Pre-treatment neutrophil to lymphocyte ratio as a predictive marker for pathological response to preoperative chemoradiotherapy in pancreatic cancer. Oncol Lett. 2016; 11(2):1560–1566. [PubMed: 26893780]
50. Benson DD, Kelher MR, Meng X, Fullerton DA, Lee JH, Silliman CC, Barnett CC. Gender-specific transfusion affects tumor-associated neutrophil: macrophage ratios in murine pancreatic adenocarcinoma. J Gastrointest Surg. 2010; 14(10):1560–1565. [PubMed: 20835771]
51. Templeton AJ, McNamara MG, Šeruga B, Vera-Badillo FE, Aneja P, Ocaña A, Leibowitz-Amit R, Sonpavde G, Knox JJ, Tran Ben, Tannock IF, Amir E. Prognostic role of neutrophil-to-lymphocyte ratio in solid tumors: a systematic review and meta-analysis. J Natl Cancer Inst. 2014; 106(6):dju124. [PubMed: 24875653]
52. Bajwa A, Kinsey GR, Okusa MD. Immune mechanisms and novel pharmacological therapies of acute kidney injury. Curr Drug Targets. 2009; 10(12):1196–1204. [PubMed: 19715538]
53. Barton GM. A calculated response: control of inflammation by the innate immune system. J Clin Invest. 2008; 118(2):413–420. [PubMed: 18246191]
54. Medzhitov R, Janeway CA Jr. Innate immunity: the virtues of a nonclonal system of recognition. Cell. 1997; 91(3):295–298. [PubMed: 9363937]
55. Nathan C. Neutrophils and immunity: challenges and opportunities. Nat Rev Immunol. 2006; 6(3): 173–182. [PubMed: 16498448]

56. Lawrence T, Willoughby DA, Gilroy DW. Anti-inflammatory lipid mediators and insights into the resolution of inflammation. Nat Rev Immunol. 2002; 2(10):787–795. [PubMed: 12360216]
57. Chen GY, Nuñez G. Sterile inflammation: sensing and reacting to damage. Nat Rev Immunol. 2010; 10(12):826–837. [PubMed: 21088683]
58. Shi C, Pamer EG. Monocyte recruitment during infection and inflammation. Nat Rev Immunol. 2011; 11(11):762–774. [PubMed: 21984070]
59. Serhan CN, Savill J. Resolution of inflammation: the beginning programs the end. Nat Immunol. 2005; 6(12):1191–1197. [PubMed: 16369558]
60. Serhan CN. Resolution phase of inflammation: novel endogenous anti-inflammatory and proresolving lipid mediators and pathways. Annu Rev Immunol. 2007; 25(1):101–137. [PubMed: 17090225]
61. Ueha S, Shand FHW, Matsushima K. Cellular and molecular mechanisms of chronic inflammation-associated organ fibrosis. Front Immunol. 2012; 3:71. [PubMed: 22566952]
62. Rock KL, Latz E, Ontiveros F, Kono H. The sterile inflammatory response. Annu Rev Immunol. 2010; 28(1):321–342. [PubMed: 20307211]
63. Nathan C. Points of control in inflammation. Nature. 2002
64. Murakami M, Hirano T. The molecular mechanisms of chronic inflammation development. Front Immunol. 2012; 3:323. [PubMed: 23162547]
65. Anderson JM, Rodriguez A, Chang DT. Foreign body reaction to biomaterials. Semin Immunol. 2008; 20(2):86–100. [PubMed: 18162407]
66. Veiseh O, Doloff JC, Ma M, Vegas AJ, Tam HH, Bader AR, Li J, Langan E, Wyckoff J, Loo WS, Jhunjhunwala S, Chiu A, Siebert S, Tang K, Hollister-Lock J, Aresta-Dasilva S, Bochenek M, Mendoza-Elias J, Wang Y, Qi M, Lavin DM, Chen M, Dholakia N, Thakrar R, Lacík I, Weir GC, Oberholzer J, Greiner DL, Langer R, Anderson DG. Size- and shape-dependent foreign body immune response to materials implanted in rodents and non-human primates. Nat Mater. 2015; 14(6):643–651. [PubMed: 25985456]
67. Chen S, Jones JA, Xu Y, Low HY, Anderson JM, Leong KW. Characterization of topographical effects on macrophage behavior in a foreign body response model. Biomaterials. 2010; 31(13): 3479–3491. [PubMed: 20138663]
68. Hu WJ, Eaton JW, Ugarova TP, Tang L. Molecular basis of biomaterial-mediated foreign body reactions. Blood. 2001; 98(4):1231–1238. [PubMed: 11493475]
69. Chen J, Shetty S, Zhang P, Gao R, Hu Y, Wang S, Li Z, Fu J. Aspirin-triggered resolvin D1 down-regulates inflammatory responses and protects against endotoxin-induced acute kidney injury. Toxicol Appl Pharmacol. 2014; 277(2):118–123. [PubMed: 24709673]
70. Chiurchiù V, Leuti A, Dalli J, Jacobsson A, Battistini L, Maccarrone M, Serhan CN. Proresolving lipid mediators resolvin D1, resolvin D2, and maresin 1 are critical in modulating T cell responses. Sci Transl Med. 2016; 8(353):353ra111.
71. Amulic B, Cazalet C, Hayes GL, Metzler KD, Zychlinsky A. Neutrophil function: from mechanisms to disease. Annu Rev Immunol. 2012; 30(1):459–489. [PubMed: 22224774]
72. Brill A, Fuchs TA, Savchenko AS, Thomas GM, Martinod K, de Meyer SF, Bhandari AA, Wagner DD. Neutrophil extracellular traps promote deep vein thrombosis in mice. J Thromb Haemost. 2012; 10(1):136–144. [PubMed: 22044575]
73. Bekler A, Erbag G, Sen H, Gazi E, Ozcan S. Predictive value of elevated neutrophil-lymphocyte ratio for left ventricular systolic dysfunction in patients with non ST-elevated acute coronary syndrome. Pak J Med Sci. 2015; 31(1):159–163. [PubMed: 25878635]
74. Mantovani A, Cassatella MA, Costantini C, Jaillon S. Neutrophils in the activation and regulation of innate and adaptive immunity. Nat Rev Immunol. 2011; 11(8):519–531. [PubMed: 21785456]
75. Mócsai A. Diverse novel functions of neutrophils in immunity, inflammation, and beyond. J Exp Med. 2013; 210(7):1283–1299. [PubMed: 23825232]
76. Wilgus TA, Roy S, McDaniel JC. Neutrophils and wound repair: positive actions and negative reactions. Adv Wound Care. 2013; 2(7):379–388.
77. Dovi JV, He LK, DiPietro LA. Accelerated wound closure in neutrophil-depleted mice. J Leukoc Biol. 2003; 73(4):448–455. [PubMed: 12660219]

78. Daley JM, Thomay AA, Connolly MD, Reichner JS, Albina JE. Use of Ly6G-specific monoclonal antibody to deplete neutrophils in mice. J Leukoc Biol. 2008; 83(1):64–70. [PubMed: 17884993]

79. Muhmmed Suliman MAR, Bahnacy Juma AA, Ali Almadhani AA, Pathare AV, Alkindi SSA, Uwe Werner F. Predictive value of neutrophil to lymphocyte ratio in outcomes of patients with acute coronary syndrome. Arch Med Res. 2010; 41(8):618–622. [PubMed: 21199731]

80. Ozdemir Y, Ozdemir Y, Akin ML, Akin ML, Sucullu I, Sucullu I, Balta AZ, Balta AZ, Yucel E. Pretreatment neutrophil/lymphocyte ratio as a prognostic aid in colorectal cancer. Asian Pac J Cancer Prev. 2014; 15(6):2647–2650. [PubMed: 24761878]

81. Poludasu S, Cavusoglu E, Khan W, Marmur JD. Neutrophil to lymphocyte ratio as a predictor of long-term mortality in african americans undergoing percutaneous coronary intervention. Clin Cardiol. 2009; 32(12):E6–E10.

82. Kasuga K, Yang R, Porter TF, Agrawal N, Petasis NA, Irimia D, Toner M, Serhan CN. Rapid appearance of resolvin precursors in inflammatory exudates: novel mechanisms in resolution. J Immunol. 2008; 181(12):8677–8687. [PubMed: 19050288]

83. Segawa M, Fukada S, Yamamoto Y, Yahagi H, Kanematsu M, SATO M, ITO T, Uezumi A, Hayashi S, Miyagoesuzuki Y. Suppression of macrophage functions impairs skeletal muscle regeneration with severe fibrosis. Exp Cell Res. 2008; 314(17):3232–3244. [PubMed: 18775697]

84. Avraham-Davidi I, Yona S, Grunewald M, Landsman L, Cochain C, Silvestre JS, Mizrahi H, Faroja M, Strauss-Ayali D, Mack M, Jung S, Keshet E. On-site education of VEGF-recruited monocytes improves their performance as angiogenic and arteriogenic accessory cells. J Exp Med. 2013; 210(12):2611–2625. [PubMed: 24166715]

85. Shechter R, Miller O, Yovel G, Rosenzweig N, London A, Ruckh J, Kim KW, Klein E, Kalchenko V, Bendel P, Lira SA, Jung S, Schwartz M. Recruitment of beneficial M2 macrophages to injured spinal cord is orchestrated by remote brain choroid plexus. Immunity. 2013; 38(3):555–569. [PubMed: 23477737]

86. Ariel A, Serhan CN. New lives given by cell death: macrophage differentiation following their encounter with apoptotic leukocytes during the resolution of inflammation. Front Immunol. 2012; 3

87. Grunewald M, Avraham I, Dor Y, Bachar-Lustig E, Itin A, Yung S, Chimenti S, Landsman L, Abramovitch R, Keshet E. VEGF-induced adult neovascularization: recruitment, retention, and role of accessory cells. Cell. 2006; 124(1):175–189. [PubMed: 16413490]

88. Zemani F, Silvestre JS, Fauvel-Lafeve F, Bruel A, Vilar J, Bieche I, Laurendeau I, Galy-Fauroux I, Fischer AM, Boisson-Vidal C. Ex vivo priming of endothelial progenitor cells with SDF-1 before transplantation could increase their proangiogenic potential. Arterioscler Thromb Vasc Biol. 2008; 28(4):644–650. [PubMed: 18239152]

89. Jenkins SJ, Ruckerl D, Cook PC, Jones LH, Finkelman FD, van Rooijen N, MacDonald AS, Allen JE. Local macrophage proliferation, rather than recruitment from the blood, is a signature of TH2 inflammation. Science. 2011; 332(6035):1284–1288. [PubMed: 21566158]

90. Goh YPS, Goh Y, Henderson NC, Henderson NC, Heredia JE, Heredia JE, Red Eagle A, Odegaard JI, Lehwald N, Nguyen KD, Sheppard D, Mukundan L, Locksley RM, Chawla A. Eosinophils secrete IL-4 to facilitate liver regeneration. Proc Natl Acad Sci USA. 2013; 110(24):9914–9919. [PubMed: 23716700]

Statement of Significance

This work is motivated by our efforts to explore the underlying mechanisms of inflammation resolution after injury and to develop biomaterial-based approaches to amplify endogenous mechanisms of resolution and repair. Though specific lipid mediators have been identified that actively promote the resolution of inflammation, biomaterial-based localized delivery of these mediators has been largely unexplored. We loaded Aspirin-Triggered Resolvin D1 into a PLGA scaffold and examined the effects of sustained, localized delivery on the innate immune response. We found that biomaterial delivery of resolvin was able to enhance the accumulation of pro-regenerative populations of immune cells, including antiinflammatory monocytes, population that has never before been shown to respond to resolvin treatment, and also enhance vascular remodeling in response to tissue injury.

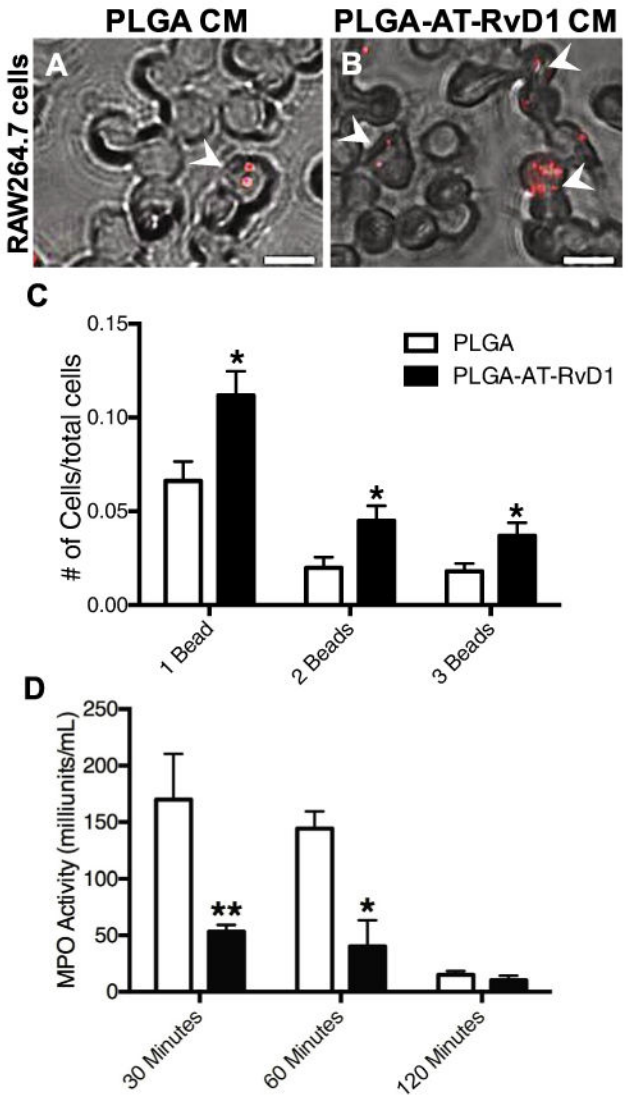

Fig. 1.

Released AT-RvD1 promotes macrophage phagocytosis and inhibits neutrophil myeloperoxidase (A-B) Brightfield and epifluorescence micrographs of RAW264.7 macrophages treated with PLGA film-conditioned media (PLGA CM) or AT-RvD1 conditioned media (PLGA-AT-RvD1 CM). White arrowheads indicate engulfed beads by macrophages. Scale bar, 5 mm (C) Quantification of phagocytic activity of RAW264.7 macrophages. (D) Myeloperoxidase activity of MPRO-differentiated neutrophils decreases significantly after treatment with AT-RvD1 conditioned media. Data presented as mean ± S.E.M. Statistical analyses were performed using two-tailed t-tests *$p < 0.05$, **$p < 0.01$ n = 3 samples per group.

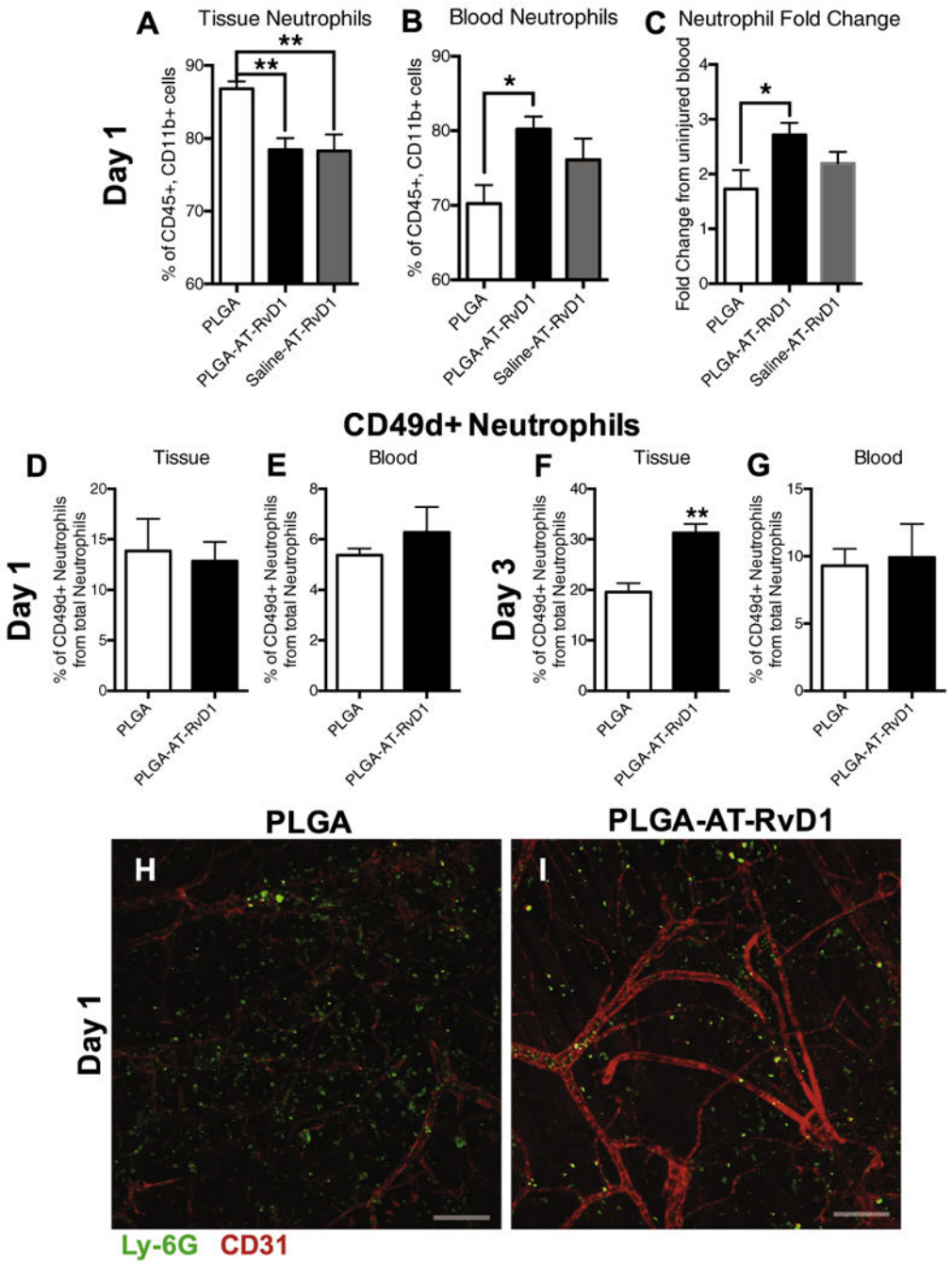

Fig. 2.

AT-RvD1 treatment sequesters neutrophils in the blood compartment after 1 day. Flow cytometric analysis of neutrophils after 1 day in the (A) blood and (B) tissue. (C) Fold change in blood neutrophils after 1 day compared to blood from an uninjured mouse. (D-G) Analysis of CD49d+ neutrophils in tissue and blood at 1 and 3 days after film implantation (H-I) Whole mount immunostaining of Ly-6G+ neutrophil infiltration into tissue one day after PLGA or AT-RvD1-loaded PLGA film implant. Scale bars, 100 μm. Data presented as

mean ± S.E.M. Statistical analyses were performed using one-way ANOVA with Tukey's post-hoc test *$p < 0.05$, **$p < 0.01$ n = 4–6 animals per group.

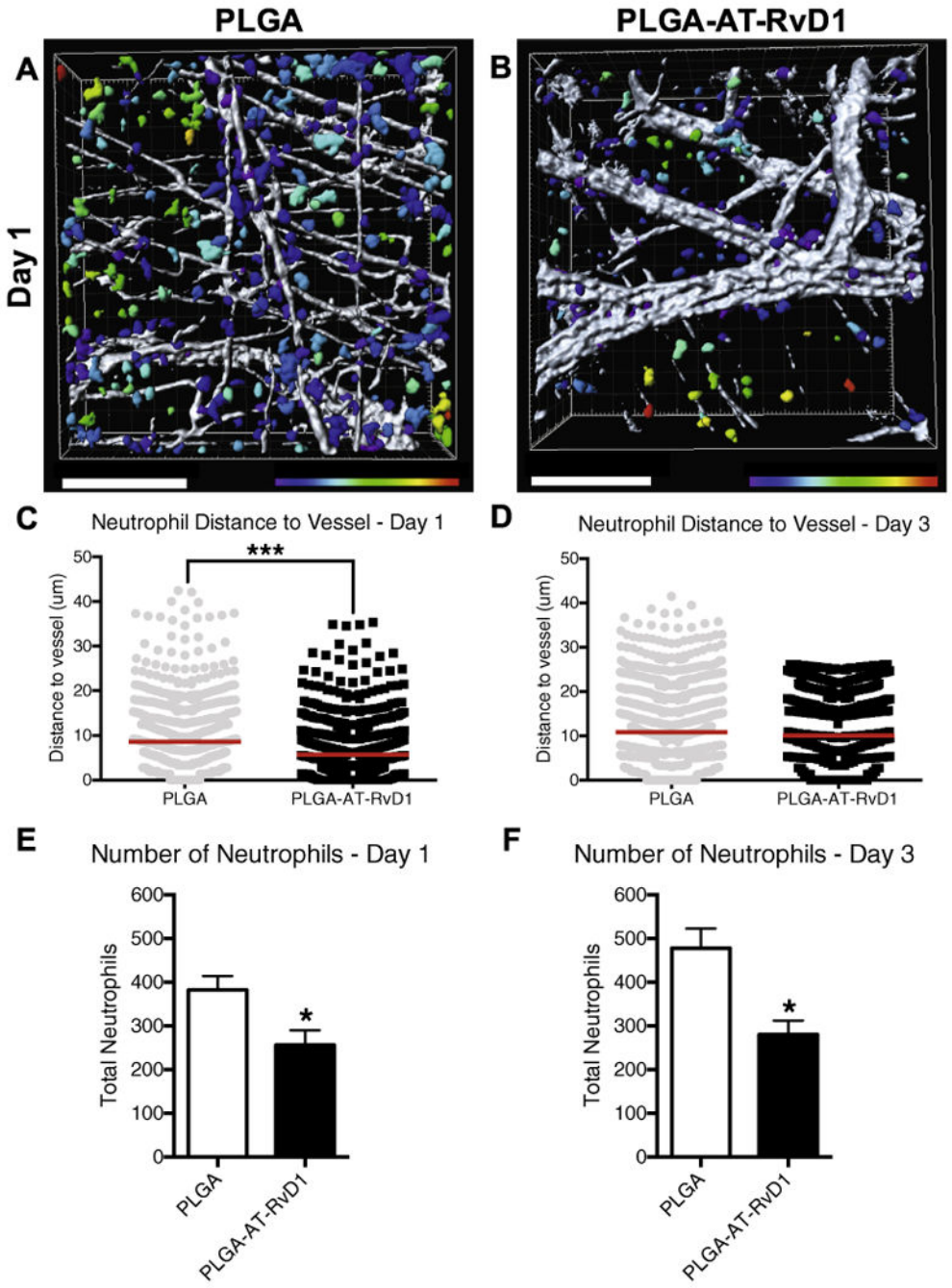

Fig. 3.

Localized AT-RvD1 delivery limits neutrophil migration through inflamed dorsal tissue. (A-B) Renderings of neutrophil distance from CD31+ vasculature one day after film implantation (representative Imaris renderings of Ly-6G+ cells, color-coded according to distance from the closest CD-31+ blood vessel: purple = 0 μm, red = 30 μm) (C-D) Quantification of neutrophil distance to vessel at post-implant days 1 and 3. Imaris 3-d quantification of neutrophil numbers after (E) one day and (F) three days. Statistical analyses were conducted using two-tailed Mann-Whitney test (C-D) and two-tailed t-test (E-

F) *p < 0.05, ***p < 0.001, n > 100 cells, across 3–4 animals per group. Scale bars, 100 mm. (For interpretation of the references to color in this figure legend, the reader is referred to the web version of this article.)

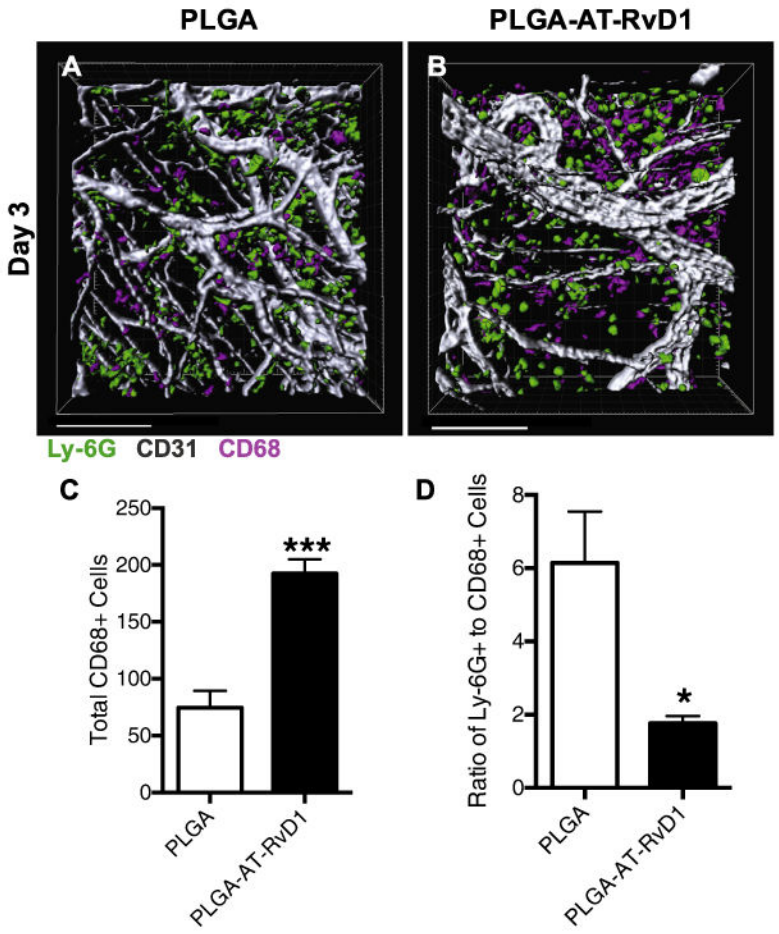

Fig. 4.

Local delivery of AT-RvD1 increases CD68+ monocytes and macrophages. (A-B) Imaris renderings of CD68+ macrophage and Ly-6G+ neutrophil accumulation. (C) Quantification of CD68+ cells found in each Imaris rendering after 3 days. (D) Neutrophil to monocyte/macrophage ratio. Scale bars, 100 μm. Data presented as mean ± S.E.M. Statistical analyses were performed using two-tailed t-test *$p < 0.05$, ***$p < 0.001$, $n > 100$ cells, across 3–4 animals per group.

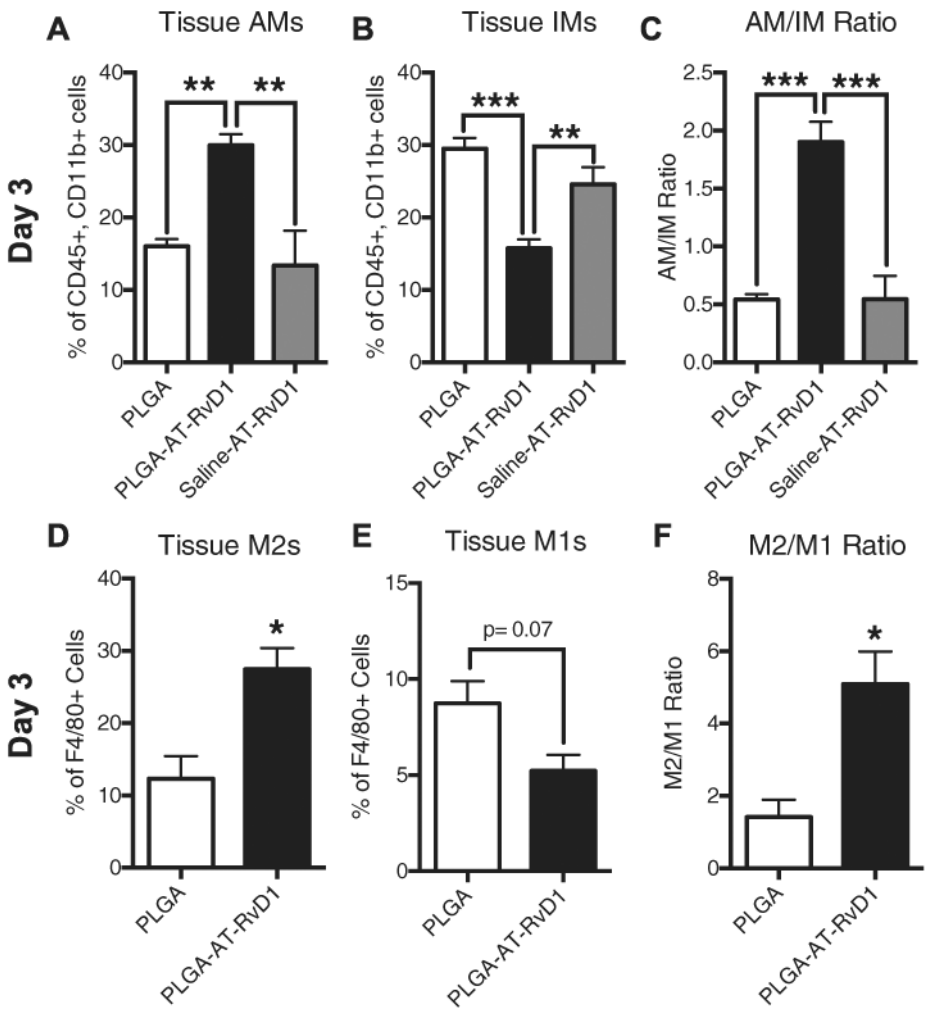

Fig. 5.

Biomaterial delivery of AT-RvD1 promotes AM and CD206+ macrophage accumulation. Flow cytometric analysis of (A) Ly-6C^{Lo} AMs and (B) Ly-6C^{Hi} IMs. (C) Tissue AM/ IM ratio. Analysis of (D) M2 (F4/80^{+} CD206^{+} CD86~) macrophages and (E) M1 (F4/80^{+} CD206^{-} CD86^{+}) macrophages at day 3. (F) M2/M1 “regenerative ratio” analysis. Data presented as mean± S.E.M. Statistical analyses were performed using one-way ANOVA with Tukey's post-hoc test or two-tailed *t*-test *p < 0.05, **p < 0.01, ***p < 0.001 n = 4-6 animals per group.

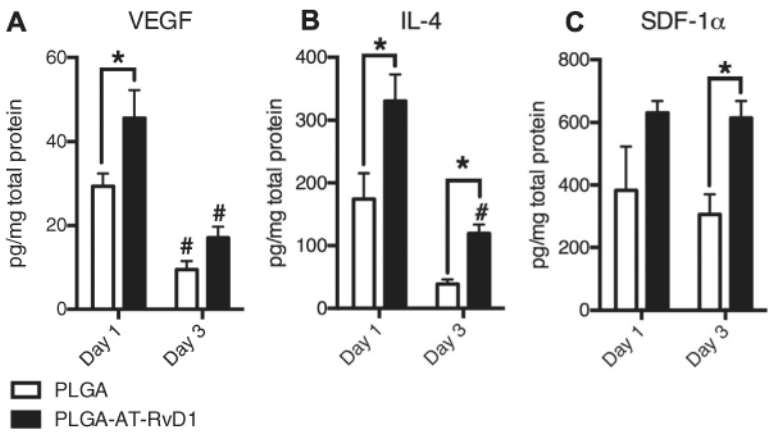

Fig. 6.

Local delivery of AT-RvD1 modulates the peri-implant cytokine profile towards regeneration and angiogenesis. (A) VEGF expression at 1 and 3 days post film implantation. (B) IL-4 expression at 1 and 3 days post film implantation. (C) SDF-1a expression at 1 and 3 days post film implantation. Data presented as mean ± S.E.M. Statistical analyses were performed using two-way ANOVA with Tukey's post-hoc test $^{*}p < 0.05$, $^{\#}p < 0.05$ compared to day 1 expression levels n = 3 animals per group.

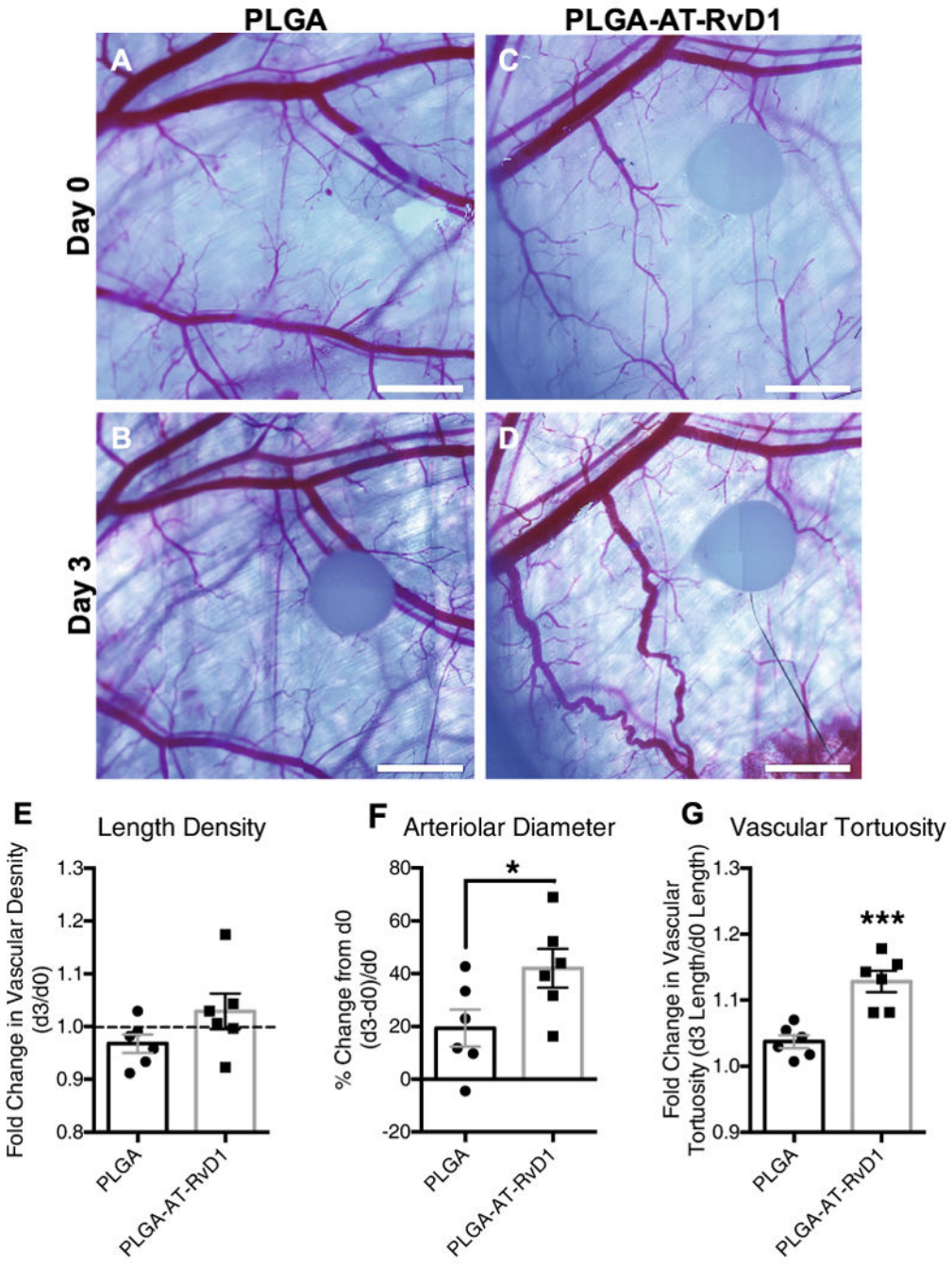

Fig. 7.

Delivery of AT-RvD1 promotes vascular remodeling. Brightfield micrographs of dorsal tissue at (A, C) day 0 and at (B, D) day 3 following treatment with AT-RvD1 loaded PLGA films. Quantification of the vascular metrics (E) length density, (F) arteriolar diameter, and (G) tortuosity. Data presented as mean ± S.E.M. Statistical analyses were performed using two-tailed *t*-tests *$p < 0.05$, ***$p < 0.001$ n = 6 animals per group. Scale bars, 1 mm.

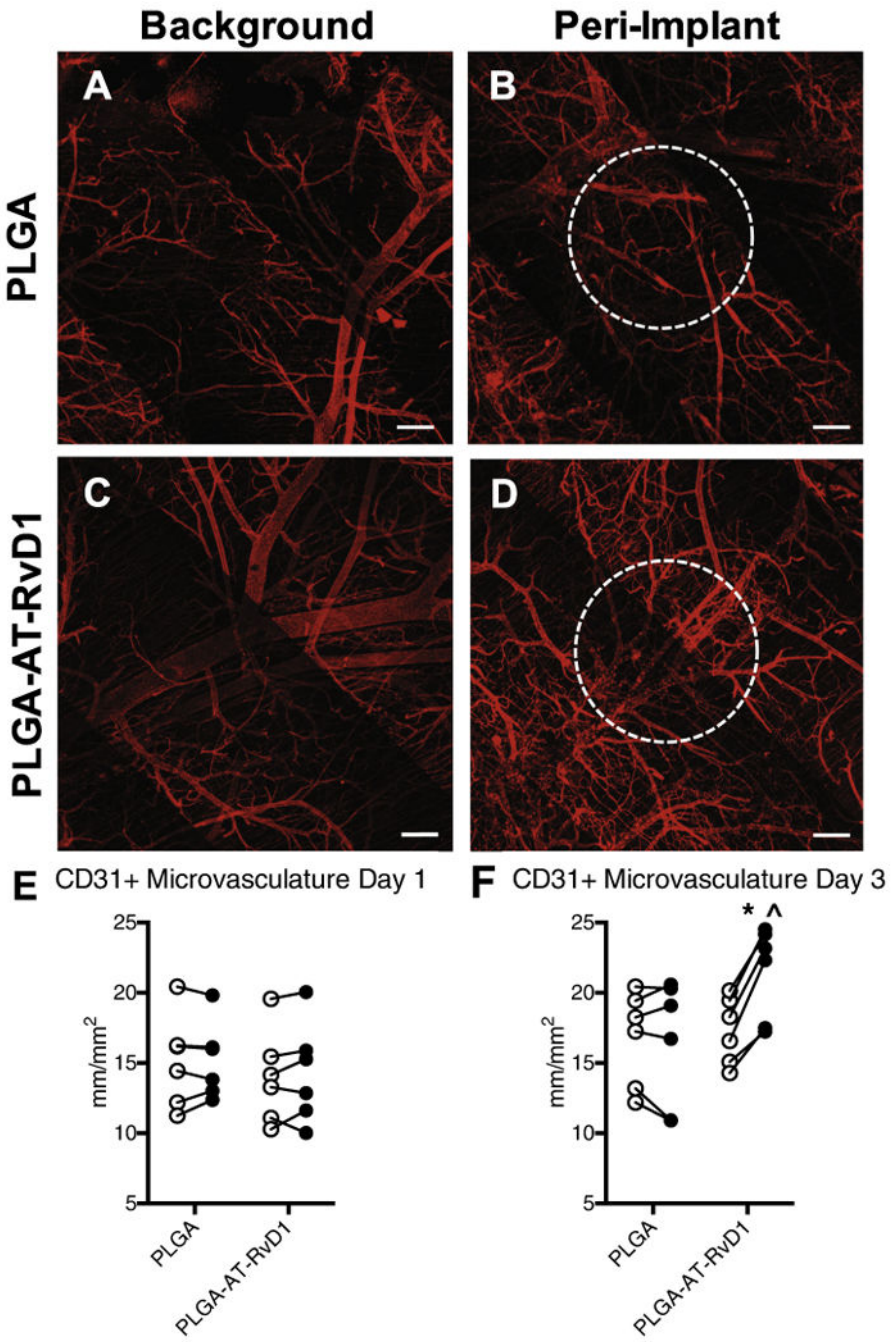

Fig. 8.

AT-RvD1 delivery enhances growth of CD31+ microvasculature. Whole mount confocal images of dorsal tissue at day 3 following treatment with AT-RvD1-loaded PLGA films. (A, C) Background microvasculature and peri-implant vasculature treated with (B) PLGA films and (D) AT-RvD1-loaded films. Quantification of microvascular length density at (E) day 1 and (F) day 3 after film implantation. ○ = background vasculature, ● = peri-implant vasculature. Statistical analysis was performed using Repeated Measures two-way ANOVA with Sidak's post-hoc test for multiple comparisons *$p < 0.05$ compared to background, ^$p <$

0.05 compared to PLGA implant, n = 6, lines connect paired analysis of background and peri-implant vasculature in each animal. Scale bars, 100 μm.